Figures and figure supplements

Robust cullin-RING ligase function is established by a multiplicity of poly-ubiquitylation pathways
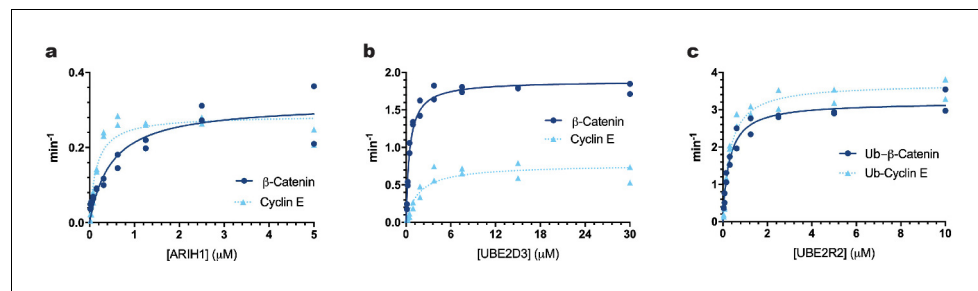
Spencer Hill *et al*

Figure 1. The K_m values of ARIH1, UBE2D3, or UBE2R2 for β-Catenin and Cyclin E peptide substrates were estimated for comparison with their physiological concentrations. Multi-turnover ubiquitylation reactions were assembled in the presence of constant amounts of SCF^{FBW7} and ^{32}P-labeled Cyclin E peptide or SCF^{βTRCP} and ^{32}P-labeled β-Catenin peptide and increasing amounts of (**a**) ARIH1 protein (along with sufficient UBE2L3 to saturate ARIH1), (**b**) UBE2D3, or (**c**) UBE2R2. In the case of UBE2R2, mono-ubiquitylated versions of the peptide substrates were used. The enzyme concentrations have been provided in **Supplementary file 2**. Reaction velocities were calculated (see Materials and methods) and plotted as a function of the protein concentration. The data were fit to the Michaelis-Menten equation, $velocity = \frac{k_{cat}[S]}{([K_m + [S])}$, where [S] represents the substrate concentration and K_m is the Michaelis constant, using nonlinear curve fitting (Prism 8 software). All reactions were performed in duplicate technical replicates. **Figure 1—figure supplement 1** shows representative autoradiograms of the ubiquitylation reactions. The R^2 values for the fit of the data to the model have been provided in **Table 1**.
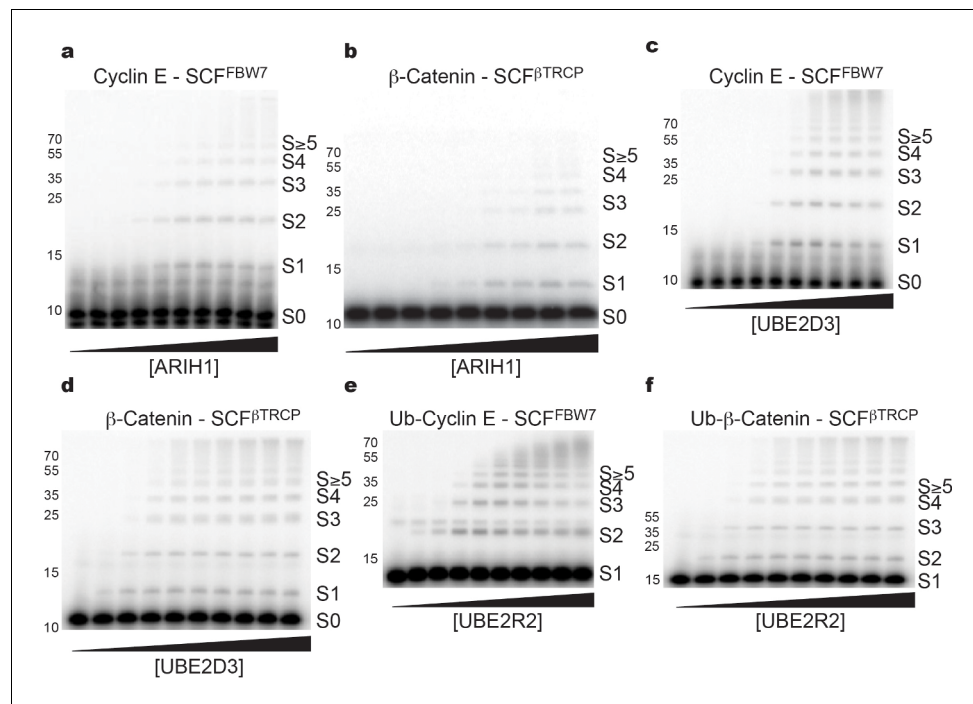
Figure 1—figure supplement 1. Autoradiograms of the ubiquitylation reactions to estimate the K_m values of ARIH1, UBE2D3, or UBE2R2 for β-Catenin and Cyclin E peptide substrates. (a) Multi-turnover ubiquitylation reactions were assembled in the presence of constant amounts of SCF^{FBW7} and ^{32}P-labeled Cyclin E peptide and increasing amounts of ARIH1 protein in combination with saturating UBE2L3. Each lane represents a single ubiquitylation reaction used to calculate the reaction velocities. (b) Same as in (a), except with β-Catenin peptide substrate and SCF^{βTRCP}. (c) Same as in (a), except with UBE2D3 protein. (d) Same as in (b), except with UBE2D3. (e) Same as in (a), except with UBE2R2 protein and mono-ubiquitylated cyclin E peptide. (f) Same as in (b), except with UBE2R2 and mono-ubiquitylated β-Catenin peptide. S0 represents unmodified substrate, S1 represents substrate modified with one ubiquitin, etc. The data are representative of duplicate technical replicates used to estimate K_m. The enzyme concentrations have been provided in *Supplementary file 2*.
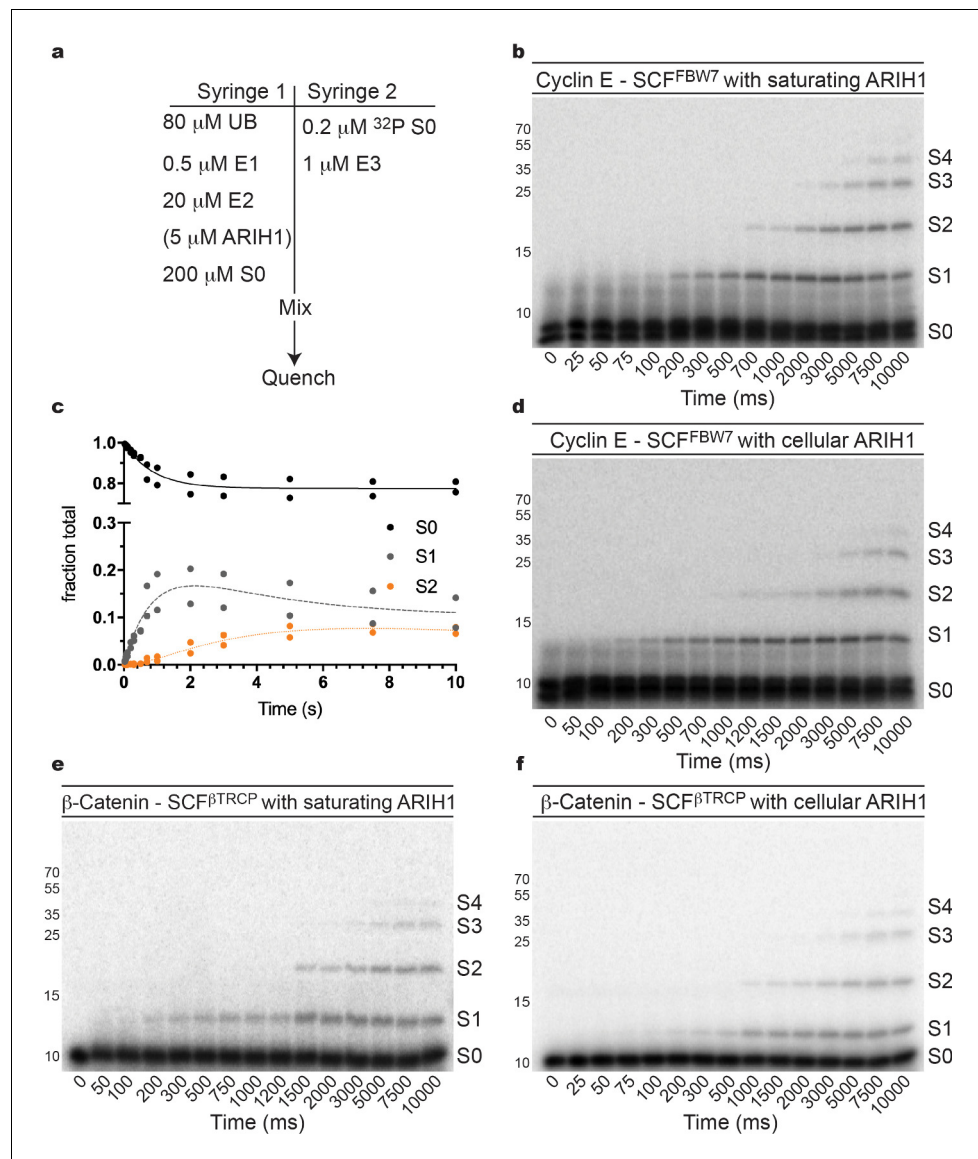
Figure 2. ARIH1 is capable of generating modest poly-ubiquitin chains onto SCF-bound substrate at either saturating or more physiological concentrations. (**a**) Typical conditions for the single-encounter quench flow ubiquitylation reactions used to estimate the rates of ubiquitin transfer. (**b**) Autoradiogram of a Cyclin E peptide ubiquitylation reaction with ARIH1 levels (2.5 µM) sufficient to saturate the SCF complex, where S0 represents unmodified substrate, S1 represents substrate modified with one ubiquitin, etc. Each time-point was performed in duplicate technical replicates. (**c**) Data points and fit to the kinetic model of the reaction in (**b**) for substrate (S0) and two products (S1 and S2). (**d**) Same as (**b**), except more physiological ARIH1 levels (*Table 2*) were used in the assay. (**e**) Same as (**b**), except with β-Catenin peptide substrate and SCF^βTRCP. (**f**) Same as (**e**), except with more physiological ARIH1 levels. *Figure 2—figure supplements 1–9* show the reactions and/or the fit of the data to the model for UBE2D3, UBE2R2, and combinations with ARIH1 or UBE2D3. The enzyme concentrations have been provided in *Supplementary file 2*.
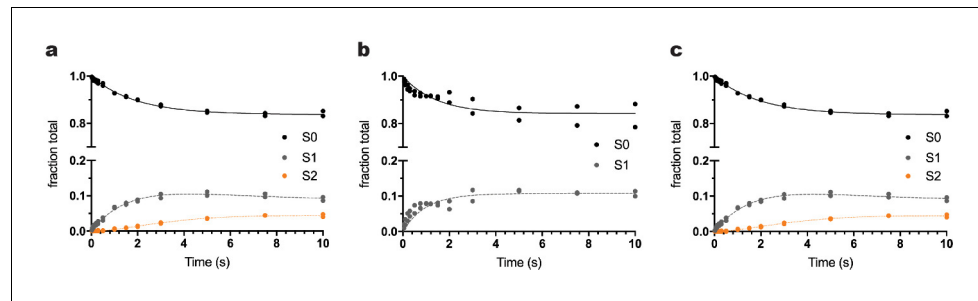
Figure 2—figure supplement 1. Estimation of the rates of ARIH1-catalyzed ubiquitin transfer to SCF-bound substrate. (a) Data points and fit to the kinetic model of a ubiquitylation reaction containing Cyclin E peptide and physiological ARIH1 levels (*Table 2*) (see *Figure 2* - panel d for the autoradiogram). Duplicate data points are shown from technical replicates. (b) Same as (a), except with β-Catenin peptide substrate levels that are saturating for SCF$^{\beta TRCP}$ (autoradiogram shown in *Figure 2* - panel e). (c) Same as (b), except with more physiological ARIH1 levels (also see *Figure 2* - panel f).
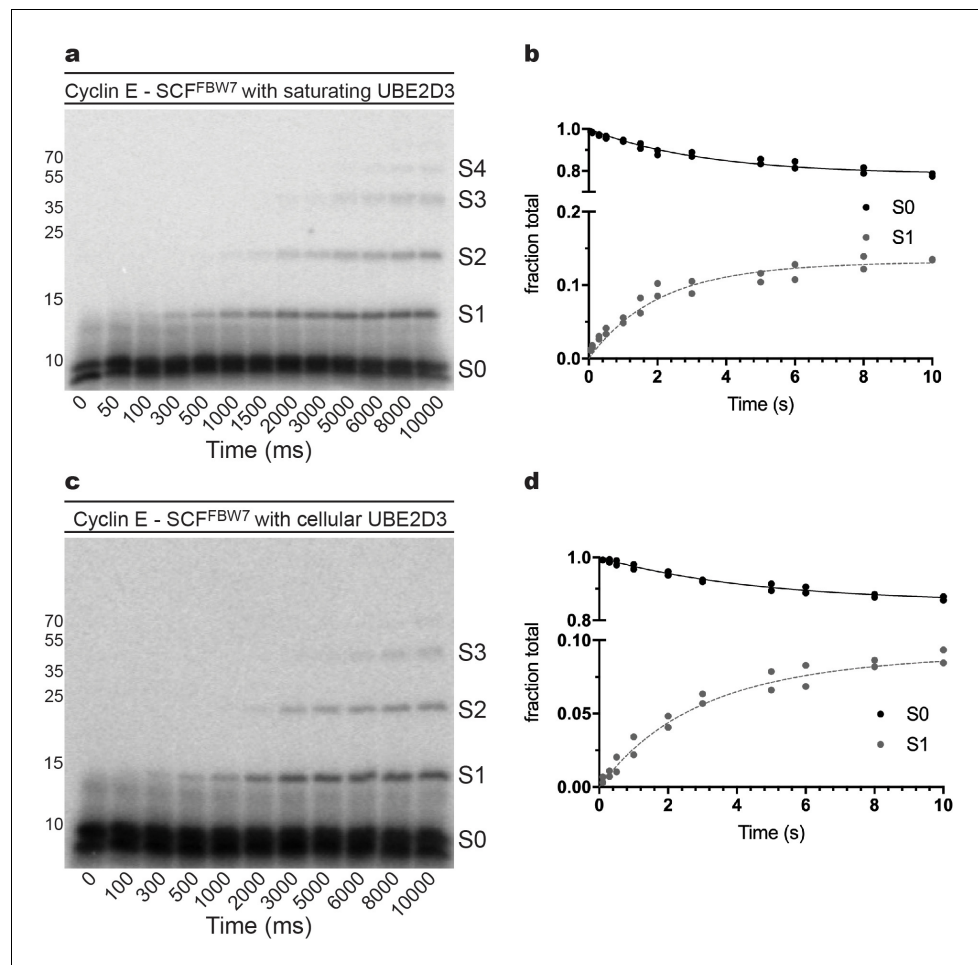
Figure 2—figure supplement 2. UBE2D3 is capable of generating modest poly-ubiquitin chains onto SCF-bound Cyclin E substrate at either saturating or more physiological concentrations. (a) Autoradiogram of a Cyclin E ubiquitylation reaction with UBE2D3 levels sufficient to saturate the SCF complex. (b) Data points and fit to the kinetic model of the reaction in (a) for substrate (S0) and mono-ubiquitylated product (S1). Duplicate data points from technical replicates are shown. (c,d) Same as (a,b), except with more physiological UBE2D3 levels. The enzyme concentrations have been provided in *Supplementary file 2*.
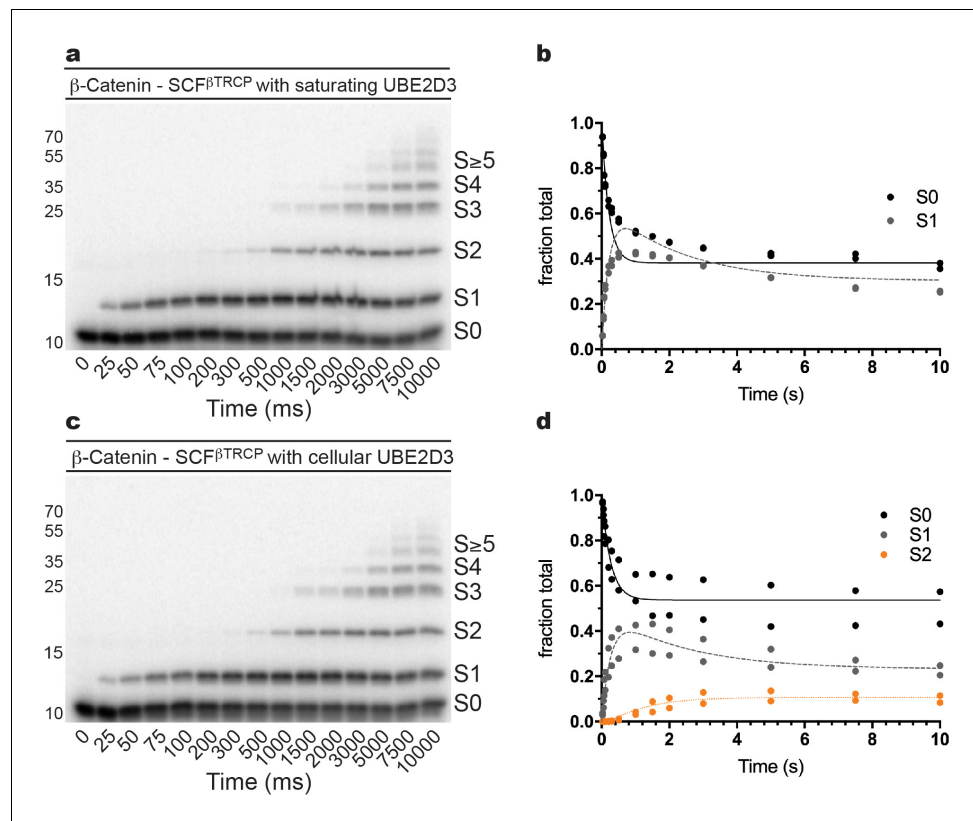
Figure 2—figure supplement 3. UBE2D3 is capable of generating modest poly-ubiquitin chains onto SCF-bound β-Catenin substrate at either saturating or more physiological concentrations. (**a**) Autoradiogram of a β-Catenin peptide ubiquitylation reaction with UBE2D3 levels sufficient to saturate the SCF complex. (**b**) Data points and fit to the kinetic model for the reaction in panel a. Duplicate data points from technical replicates are shown. (**c,d**) Same as (**a,b**), except with more physiological UBE2D3 levels. The enzyme concentrations have been provided in *Supplementary file 2*.
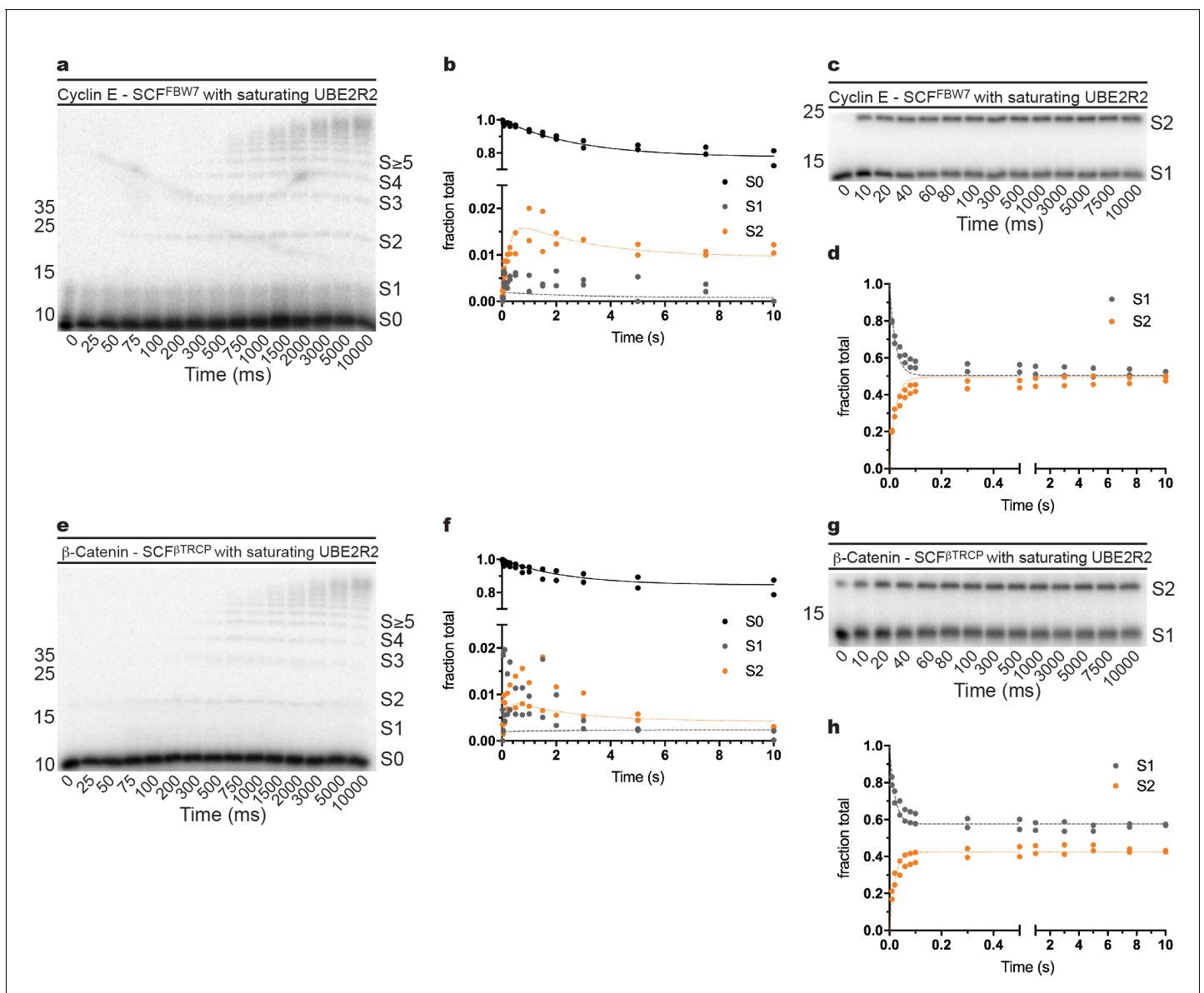
Figure 2—figure supplement 4. UBE2R2 generates robust poly-ubiquitin chains onto SCF-bound substrates when its levels are sufficient to saturate SCF. (a) Autoradiogram of a Cyclin E ubiquitylation reaction with saturating UBE2R2 levels. Notice that mono-ubiquitylated substrate (S1) is barely detectible since it is very rapidly converted to S2. (b) Data points and fit to the kinetic model for the reaction in panel a. Estimation of the rate of ubiquitin transfer from UBE2R2 ~ ubiquitin to S1 was done independently, since S1 levels are only approximately 1% of the total signal and could not be reliably fit to the model. Duplicate data points from technical replicates are shown. (c) Autoradiogram of a mono-ubiquitylated Cyclin E peptide (S1) ubiquitylation reaction containing SCF^{FBW7} and saturating levels of UBE2R2. Reactions were also carried out in the presence of lysine-less (K0) ubiquitin, resulting in a single product (S2). (d) Data points and fit to the single, exponential decay of S1 and the formation of S2 from the reaction in panel c. Duplicate data points from technical replicates are shown. (e, f) Same as in (a, b), except with β-Catenin peptide substrate and SCF^{βTRCP}. (g, h) Same as in (c, d), except with mono-ubiquitylated β-Catenin peptide substrate and SCF^{βTRCP}. The enzyme concentrations have been provided in *Supplementary file 2*.
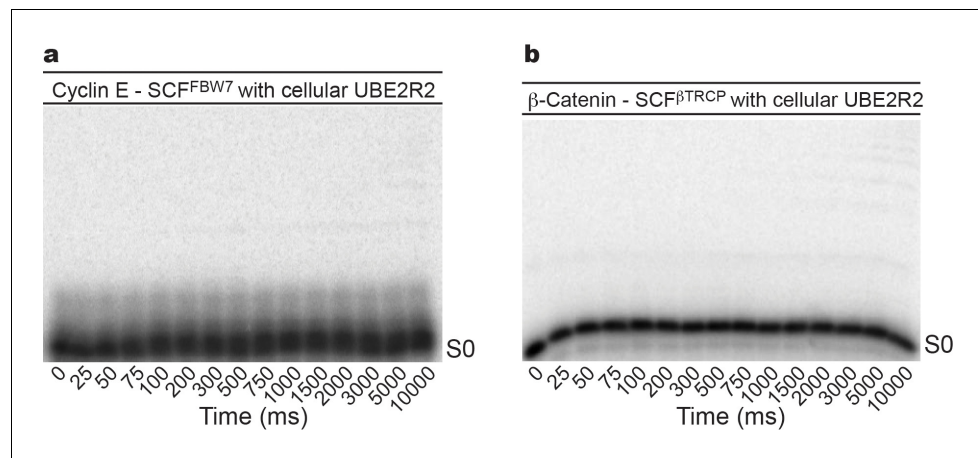
Figure 2—figure supplement 5. UBE2R2 activity is negligible when assayed at physiological conditions. (a) Autoradiogram of a Cyclin E ubiquitylation reaction with more physiological UBE2R2 levels. (b) Same as in (a), except with β-Catenin peptide substrate and SCF^{βTRCP}. The data are representative of duplicate technical replicates. The enzyme concentrations have been provided in *Supplementary file 2*.
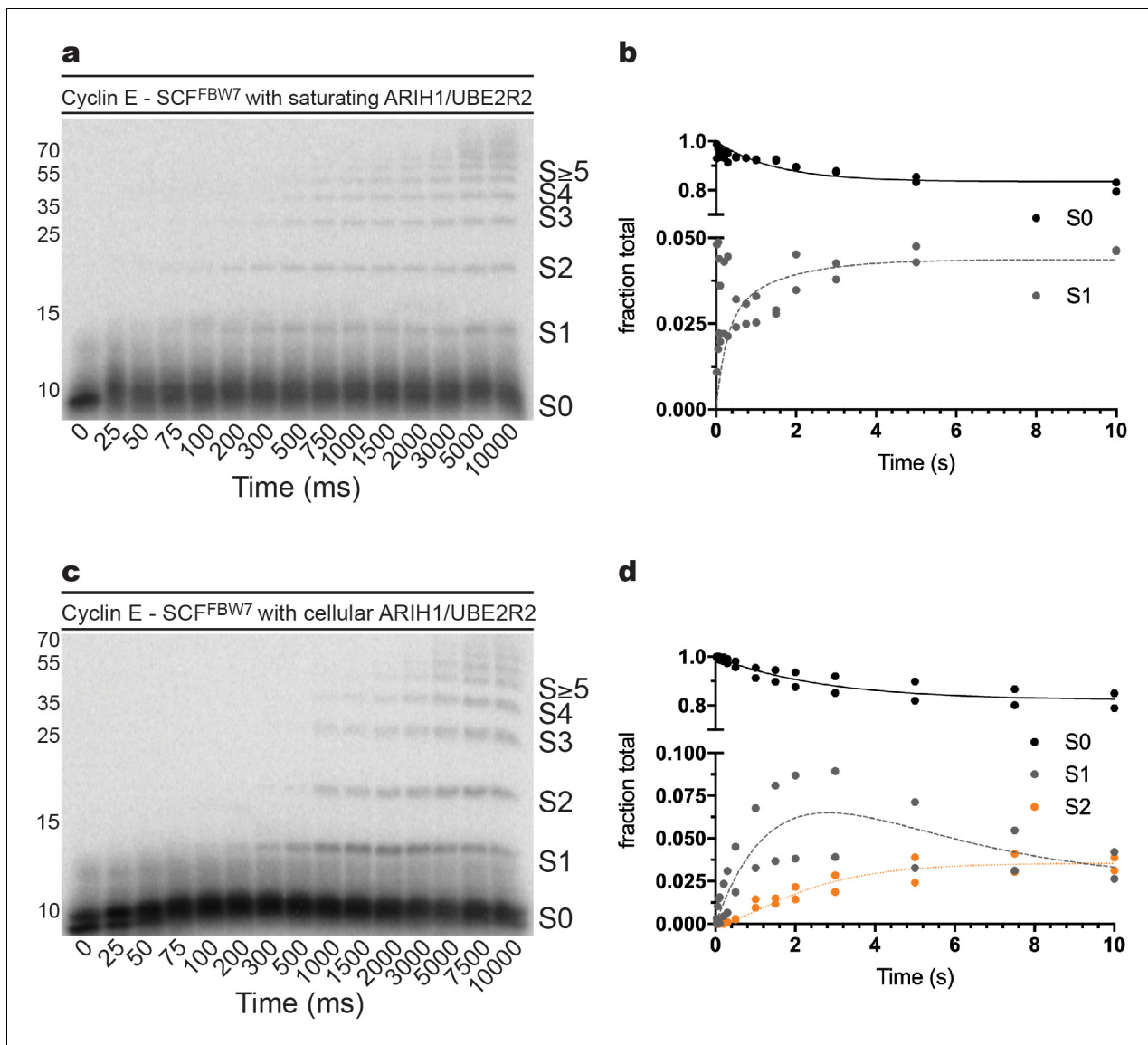
Figure 2—figure supplement 6. The combination of ARIH1 with UBE2R2 protein results in Cyclin E substrates modified with longer poly-ubiquitin chains than with ARIH1 alone. (a) Autoradiogram of a Cyclin E ubiquitylation reaction with ARIH1 and UBE2R2 levels sufficient to saturate the SCF complex. (b) Data points and fit to the kinetic model for the reaction shown in panel a. Duplicate data points from technical replicates are shown. (c, d) Same as (a, b), except with more physiological ARIH1 and UBE2R2 levels. The enzyme concentrations have been provided in *Supplementary file 2*.
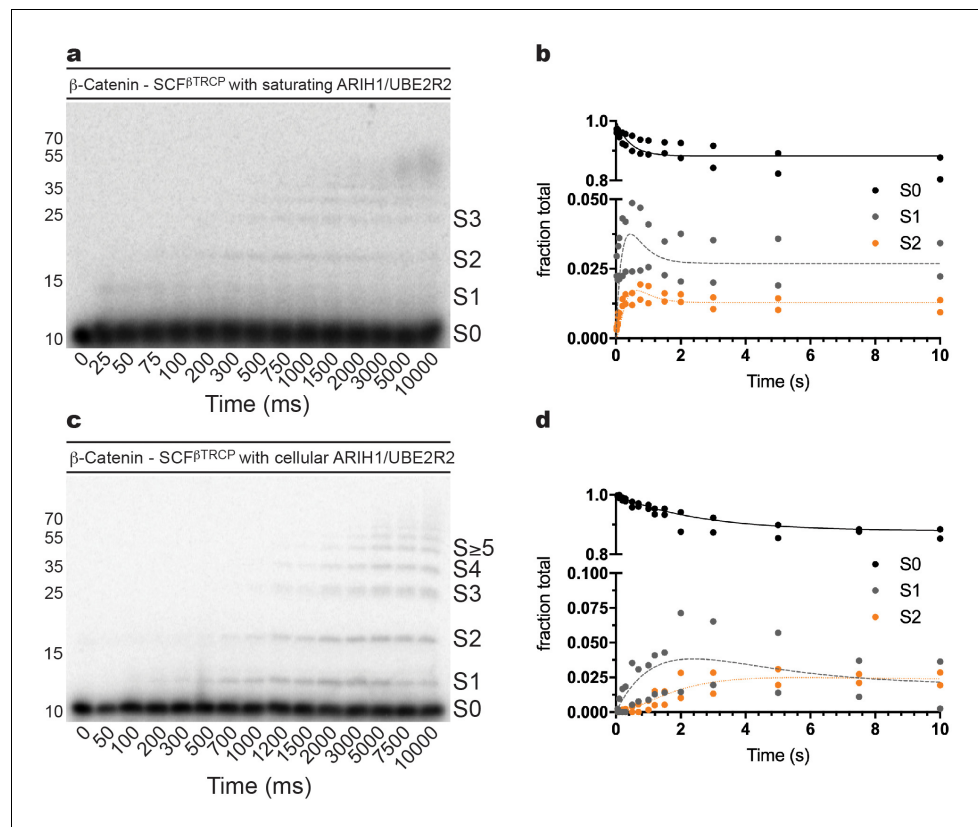
Figure 2—figure supplement 7. The combination of ARIH1 with UBE2R2 protein results in β-Catenin substrates modified with longer poly-ubiquitin chains than with ARIH1 alone. (**a**) Autoradiogram of a β-Catenin peptide ubiquitylation reaction with ARIH1 and UBE2R2 levels sufficient to saturate the SCF complex. (**b**) Data points and fit to the kinetic model for the reaction in panel a. Duplicate data points from technical replicates are shown. (**c, d**) Same as (**a, b**), except with more physiological ARIH1 and UBE2R2 levels. The enzyme concentrations have been provided in *Supplementary file 2*.
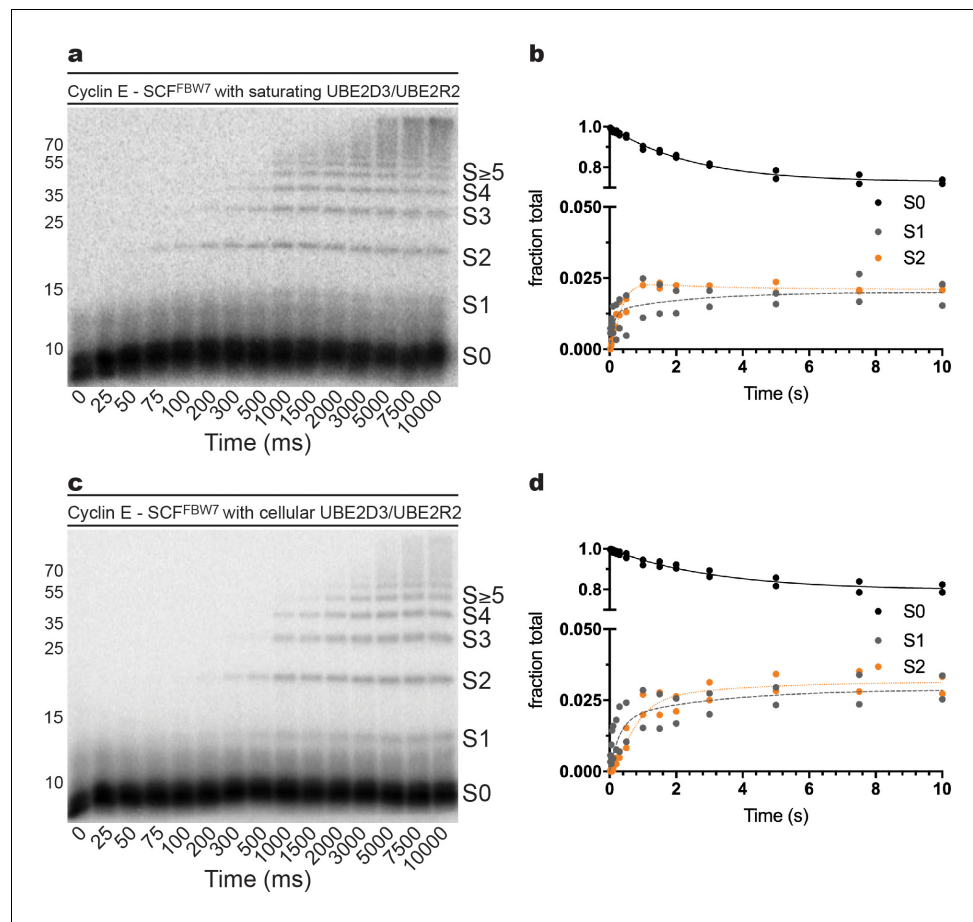
Figure 2—figure supplement 8. The combination of UBE2D3 with UBE2R2 protein results in substrates modified with longer poly-ubiquitin chains than with UBE2D3 alone. (a) Autoradiogram of a Cyclin E ubiquitylation reaction with UBE2D3 and UBE2R2 levels sufficient to saturate the SCF complex. (b) Data points and fit to the kinetic model for the reaction in panel a. Duplicate data points from technical replicates are shown. (c, d) Same as (a, b) except with more physiological UBE2D3 and UBE2R2 levels. The enzyme concentrations have been provided in *Supplementary file 2*.
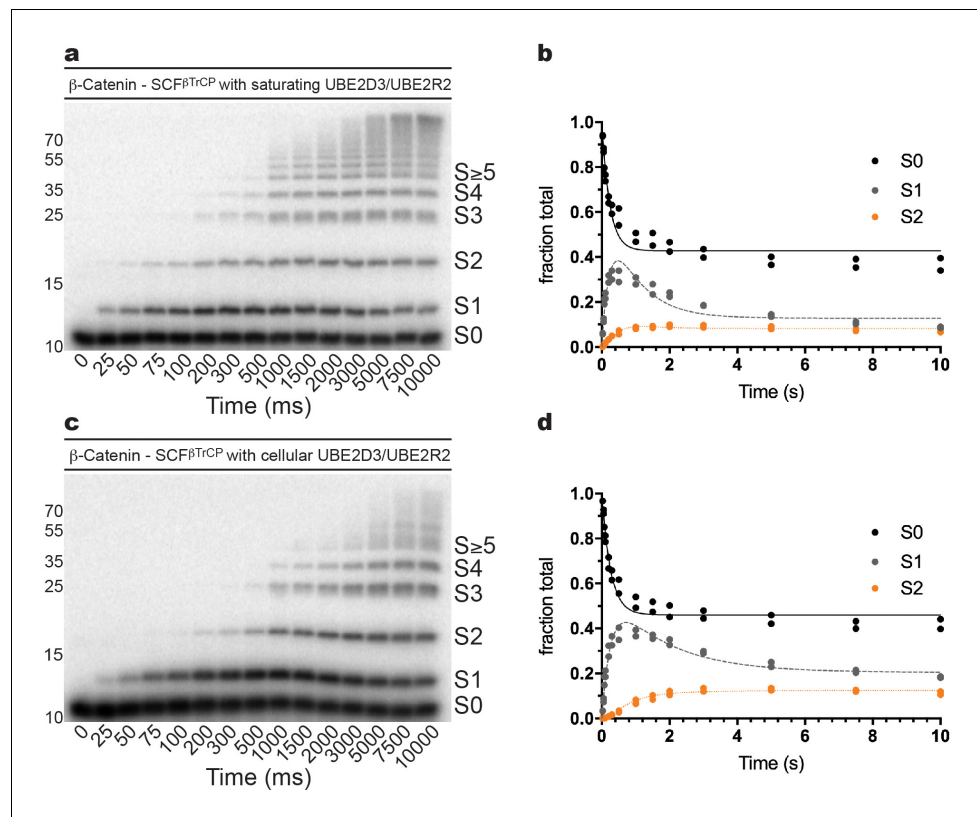
Figure 2—figure supplement 9. The combination of UBE2D3 with UBE2R2 protein results in substrates modified with longer poly-ubiquitin chains than with UBE2D3 alone, especially in the presence of β-Catenin peptide substrate. (a) Autoradiogram of a β-Catenin peptide ubiquitylation reaction with UBE2D3 and UBE2R2 levels sufficient to saturate the SCF complex. (b) Data points and fit to the kinetic model for the reaction in panel a. Duplicate data points from technical replicates are shown. (c, d) Same as (a, b), except with more physiological UBE2D3 and UBE2R2 levels. The enzyme concentrations have been provided in *Supplementary file 2*.

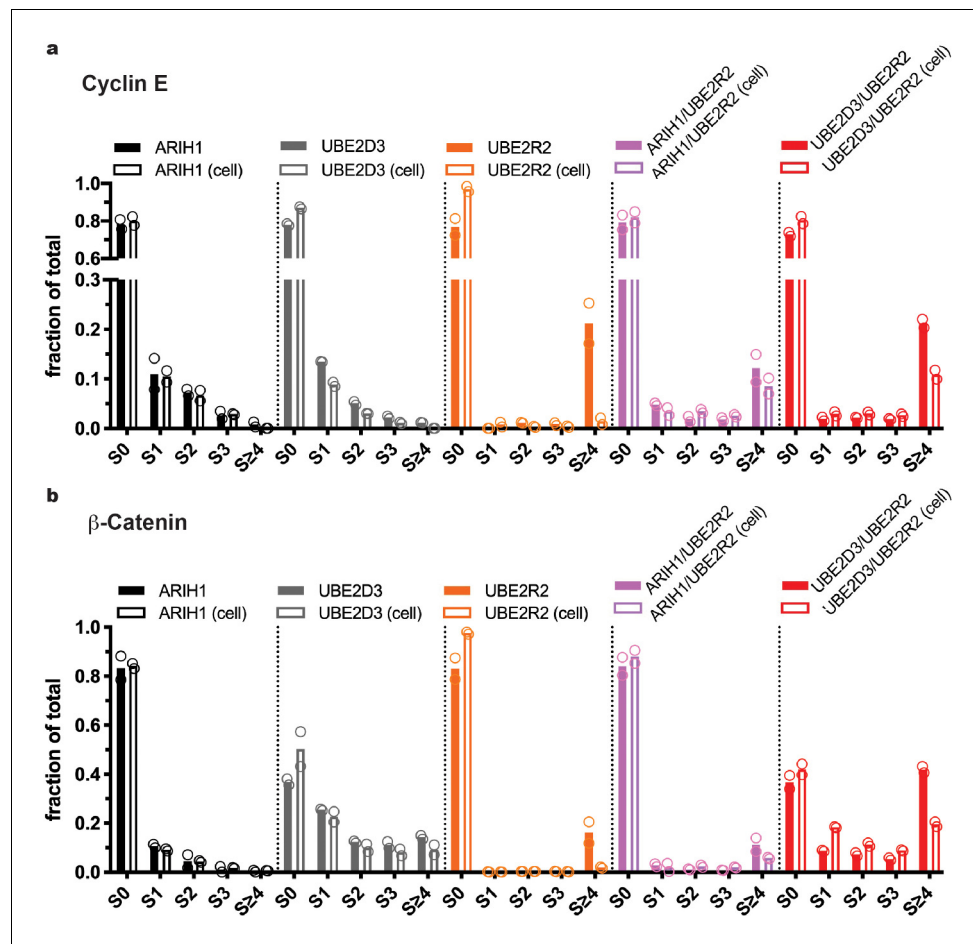**Figure 3.** Multiple routes to SCF-mediated substrate ubiquitylation. At saturating conditions, all enzymes can prime SCF-bound substrates, but only UBE2D3 and ARIH1 can prime at physiological concentrations. (a) Quantitation of the fractions of Cyclin E substrate (S0) and all products taken from the 10 s time-points from the quench flow reactions in *Figure 2*. Solid bars represent levels for reactions where ARIH1, UBE2D3, and/or UBE2R2 were saturating for SCF; empty bars represent reactions containing the same enzymes at more physiological levels (*Table 2*). Notice that UBE2R2 is capable of generating substantial products with long poly-ubiquitin chains when saturating for SCF[FBW7], but produces almost no product when UBE2R2 levels are at estimated physiological levels. (b) Same as in (a), except with β-Catenin peptide substrate and SCF[BTRCP].
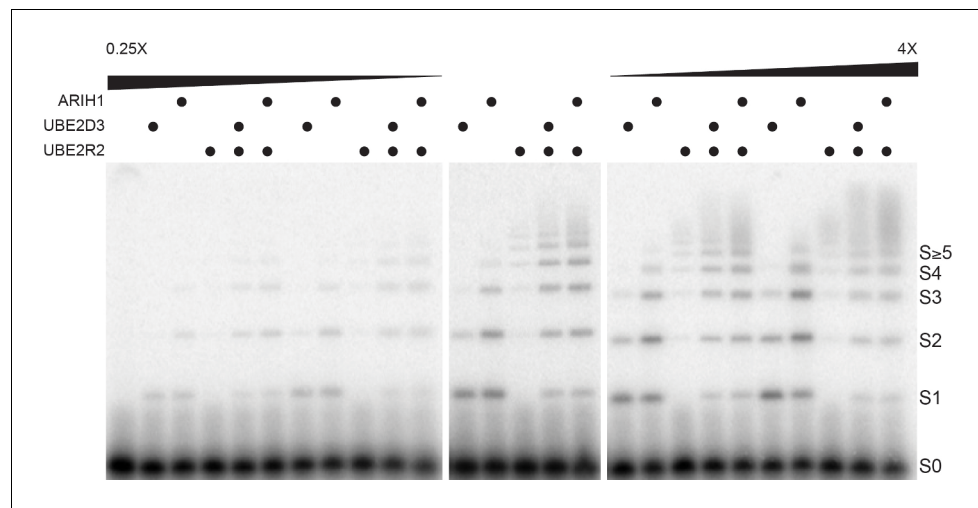
Figure 4. Altered ARIH1, UBE2D3, and/or UBE2R2 levels result in substantial differences in both the fraction of substrate converted to product as well as the average number of ubiquitins in poly-ubiquitin chains. Single-encounter ubiquitylation reactions were initiated with either ARIH1, UBE2D3, or UBE2R2 alone or relevant combinations at estimated cellular levels (middle panel). The same reactions were also performed with either a 2- or 4-fold reduction in the enzyme levels (left panel), or 2- or 4-fold greater levels (right panel). All reactions were performed in duplicate technical replicates. *Figure 4—figure supplement 1* provides graphs of the relative frequencies for the distribution of unmodified substrate and products. The enzyme concentrations have been provided in *Supplementary file 2*.
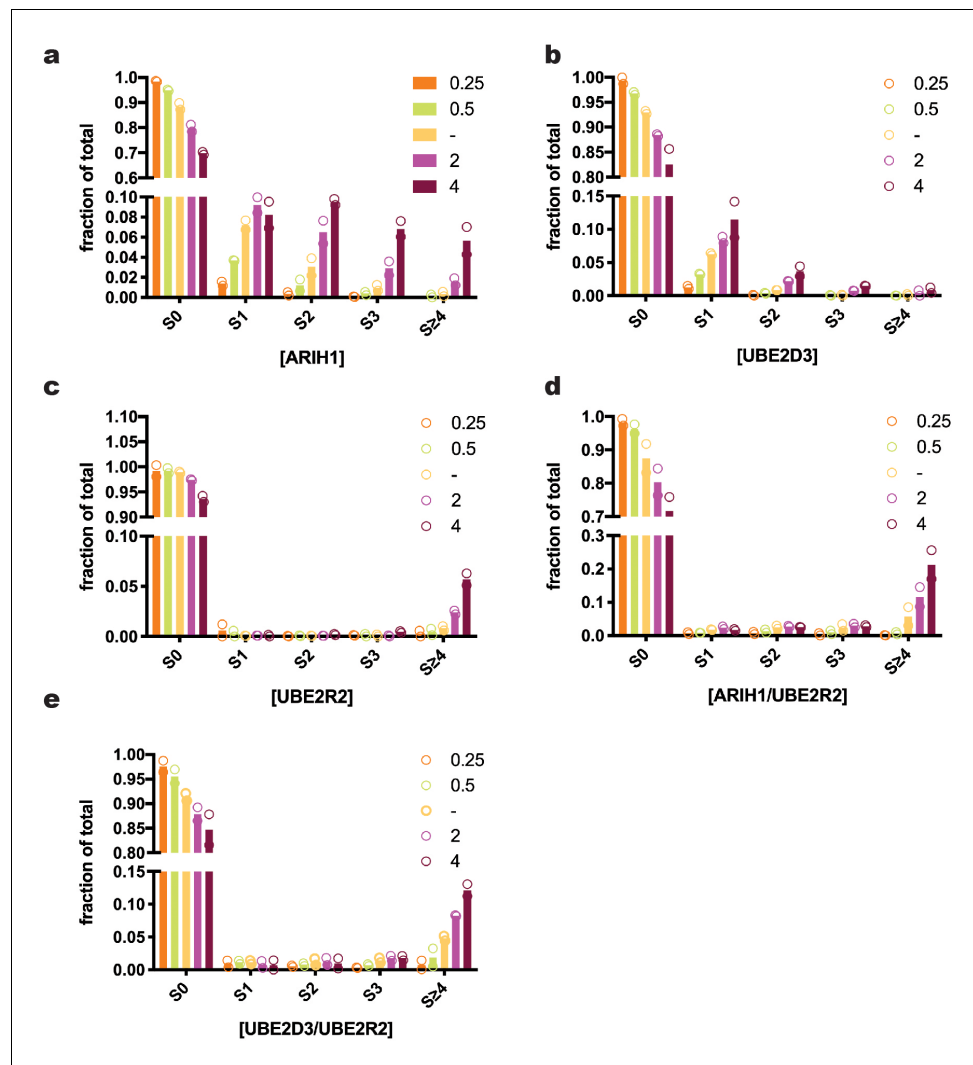
Figure 4—figure supplement 1. Modest changes to ARIH1, UBE2D3, and/or UBE2R2 levels result in substantial differences in both the fraction of substrate converted to products as well as the average number of ubiquitins in poly-ubiquitin chains. (a) Quantitation of the fractions of substrate (S0) and all products from the single-encounter reactions in *Figure 4* containing varying amounts of ARIH1 protein. The mid-range level was near physiological (*Table 2*). (b) Same as in (a), except with UBE2D3. (c) Same as in (a), except with UBE2R2. (d) Same as in (a), except with both ARIH1 and UBE2R2. (e) Same as in (a), except with both UBE2D3 and UBE2R2. Data points are shown from duplicate technical replicates.
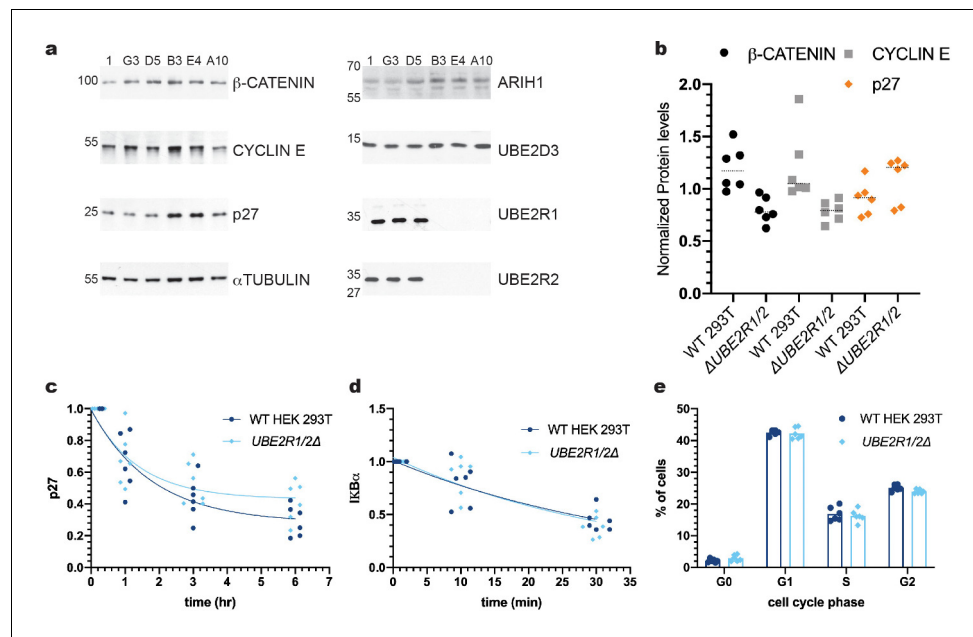
Figure 5. The ablation of both UBE2R1 and UBE2R2 proteins in cells has no effect on the stabilities of four SCF substrates nor on cell cycle progression. (a) Comparison of the steady state stabilities of β-CATENIN, CYCLIN E, and p27 proteins in either control cell lines (clones 1, G3, and D5) or *UBE2R1/2* double knockout cell lines (clones B3, E4 and A10). Demonstrations of the anti-UBE2R1 and anti-UBE2R2 antibody specificities are provided in *Figure 5—figure supplements 2* and *5b*. (b) β-CATENIN (black circles), CYCLIN E (gray squares), and p27 (orange diamonds) protein levels from control or *UBE2R1/2* double knockout cell lines. The median levels for each group are shown as dashed horizonal lines. While two of the double knockout cell lines showed evident enrichment of p27 in comparison with control cells, this result did not meet a minimal standard for statistical significance (p-value of 0.13 using an unpaired t-test). (c) Cycloheximide chase time courses measuring p27 protein stability from either control or *UBE2R1/2* double knockout cells. Protein levels were normalized to the untreated samples and fit to a one phase decay model (R^2 values for control and knockout cells were 0.85 and 0.77, respectively). Representative immunoblots are shown in *Figure 5—figure supplement 3a*. (d) TNFα-induced degradation of IκBα is comparable in either control or *UBE2R1/2* double knockout cells. Protein levels were normalized to the untreated samples and fit to a one phase decay model (R^2 values for control and double knockout cells are 0.77 and 0.80, respectively). Representative immunoblots are shown in *Figure 5—figure supplement 3b*. (e) Cell cycle analysis was performed on actively dividing populations of control or *UBE2R1/2* double knockout cells. Representative spectra are shown in *Figure 5—figure supplement 4*. Three biological replicates each for control and *UBE2R1/2* double knockout cell lines with duplicate technical replicates were used to generate the data for all panels.
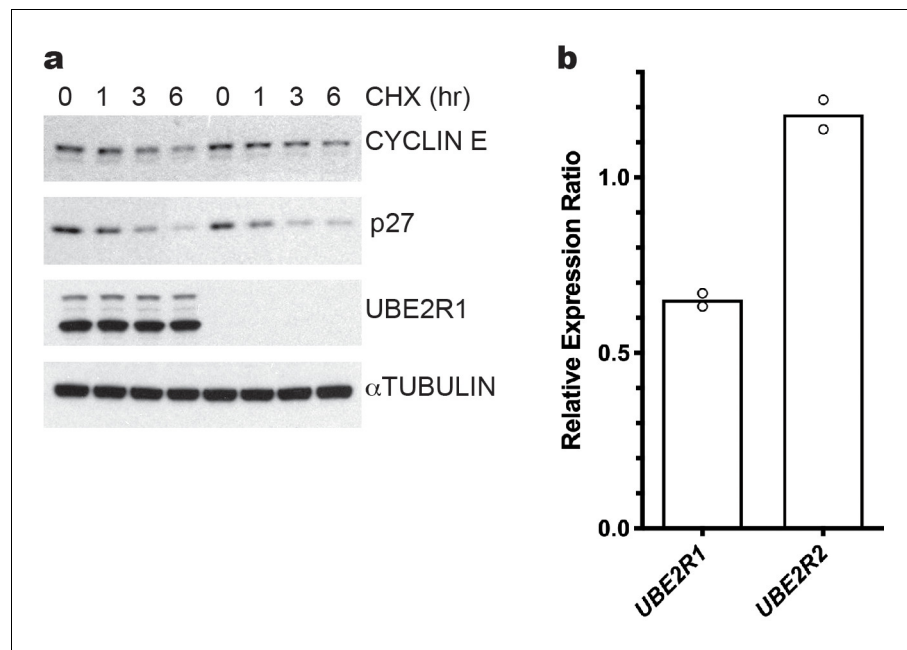
Figure 5—figure supplement 1. The ablation of UBE2R1 protein in cells has no effect on the stabilities of CYCLIN E and p27 proteins as well as *UBE2R2* expression levels. (a) Representative data showing the stabilities of CYCLIN E and p27 proteins from a cycloheximide (CHX) chase experiment comparing wild-type and *UBE2R1* knockout 293T-FiTx cells. (b) Relative expression ratios for either *UBE2R1* or *UBE2R2* mRNA comparing wild-type or *UBE2R1* knockout 293T-FiTx cells. Data points are shown from duplicate technical replicates.
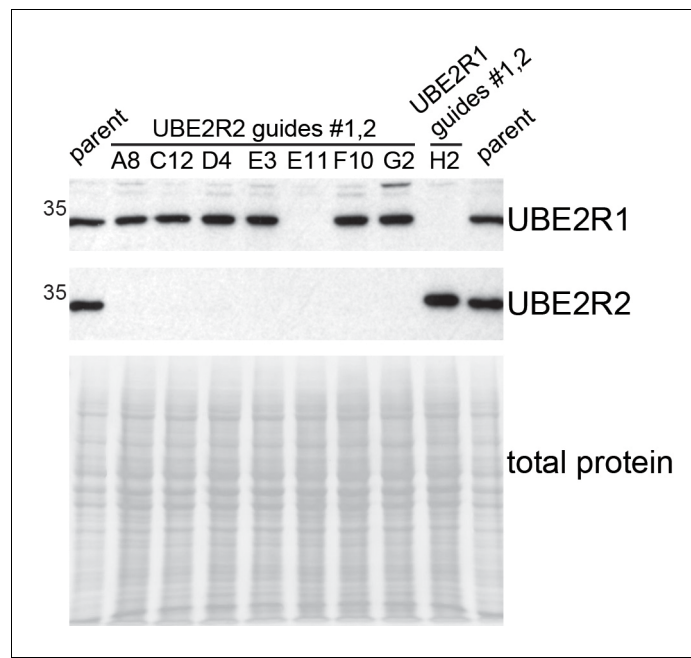
Figure 5—figure supplement 2. Antibody specificities for UBE2R1 and UBE2R2. (a) Immunoblot of cellular lysates from the parental and various *UBE2R1*, *UBE2R2* and *UBE2R1/2* knockout cell lines demonstrating the specificities of the antibodies used to detect UBE2R1 and the closely related UBE2R2 protein (greater than 85% amino acid sequence identity). Notice that colony E11 shows ablation of both *UBE2R1* and *UBE2R2*, likely due to the high similarity of *UBE2R2* guide #2 with the *UBE2R1* DNA sequence. The anti-UBE2R2 antibody was used for all immunoblots throughout the manuscript, whereas the anti-UBE2R1 antibody was used for immunoblots shown in *Figure 6—figure supplements 1* and *2*.
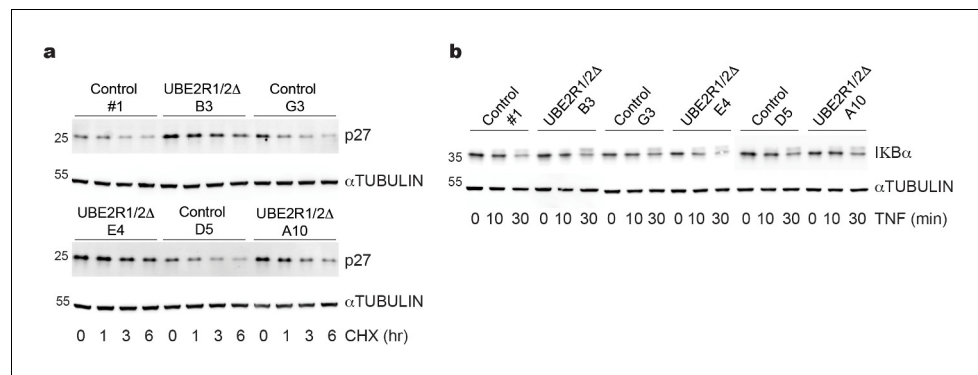
Figure 5—figure supplement 3. The rates of degradation of p27 and IκBα proteins are highly similar in control and *UBE2R1/2* knockout 293T cells. (a) Representative immunoblots for the cycloheximide chase experiment shown in *Figure 5c*. (b) Representative immunoblots for the TNFα-induced degradation of IκBα protein (*Figure 5d*). Three independent cell lines for control (clones 1, G3 and D5) and *UBE2R1/2* double knockout (clones B3, E4, and A10) cells were used to generate the data for both panels with duplicate technical replicates.
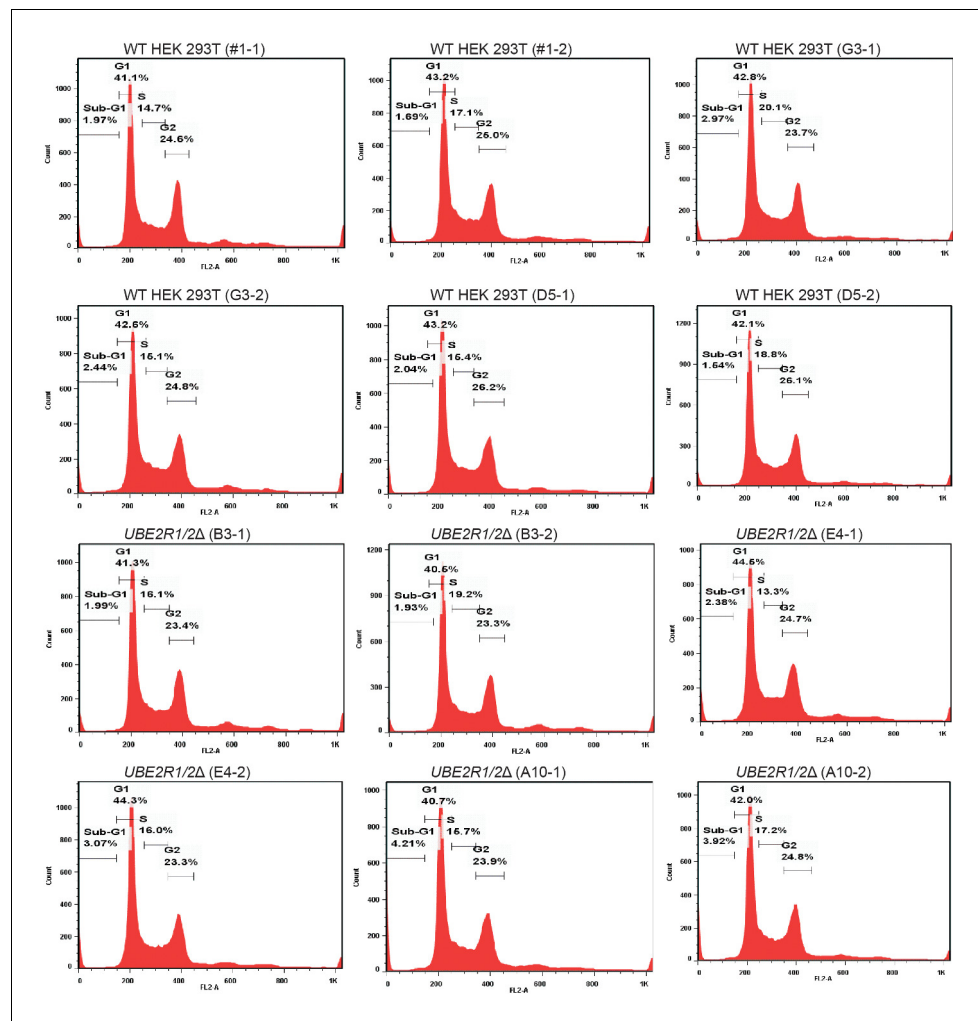
Figure 5—figure supplement 4. The ablation of UBE2R1 and UBE2R2 proteins has no effect on 293T cell cycle progression. Representative flow cytometry profiles for three control (clones 1, G3 and D5) and three *UBE2R1/2* double knockout (clones B3, E4, and A10) cell lines. Duplicate technical replicates were used to generate the graph shown in *Figure 5e*.
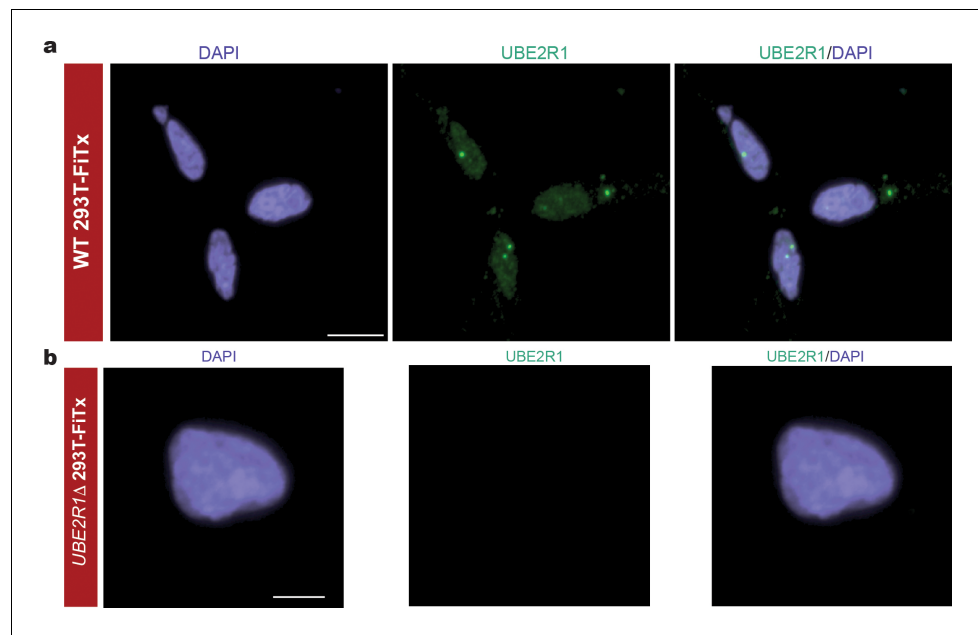
Figure 5—figure supplement 5. UBE2R1 protein is localized throughout 293T-FiTx cells. (a) Immunofluorescence staining of UBE2R1 protein (green; middle panel). UBE2R1 protein is visible with modest evident nuclear enrichment, to a lesser extent in the cytoplasm, and in adjacent pairs of foci. Scale bar, 5 μM. (b) Immunofluorescence staining for UBE2R1 protein (green; middle panel) performed on HEK 293T-FiTx *UBE2R1* knockout cells. Notice that no UBE2R1 staining is observed. Scale bar, 20 μM. Representative data are shown from duplicate biological replicates.
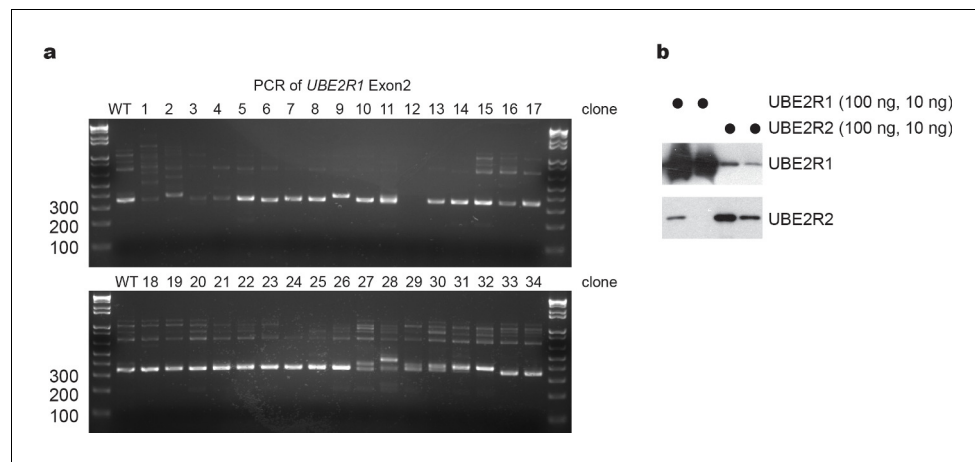
Figure 5—figure supplement 6. Generation of a *UBE2R1* knockout cell line. (**a**) Products from PCR reactions spanning the *UBE2R1* exon two guide RNA site were resolved by agarose gel electrophoresis. Incorporation of the oligo DNA (see *Supplementary file 1* - Key Resources Table) into the genome should increase the PCR product by 50 base pairs. Notice that upward shifts were observed for multiple clones, such as 9 and 32. The results are representative of duplicate technical replicates. (**b**) Demonstration of the specificity of an anti-UBE2R1 antibody with recombinant UBE2R1 and UBE2R2 proteins. This antibody was used to generate immunoblots shown in *Figure 5a*, *Figure 5—figure supplement 1*, and *Figure 7a*.
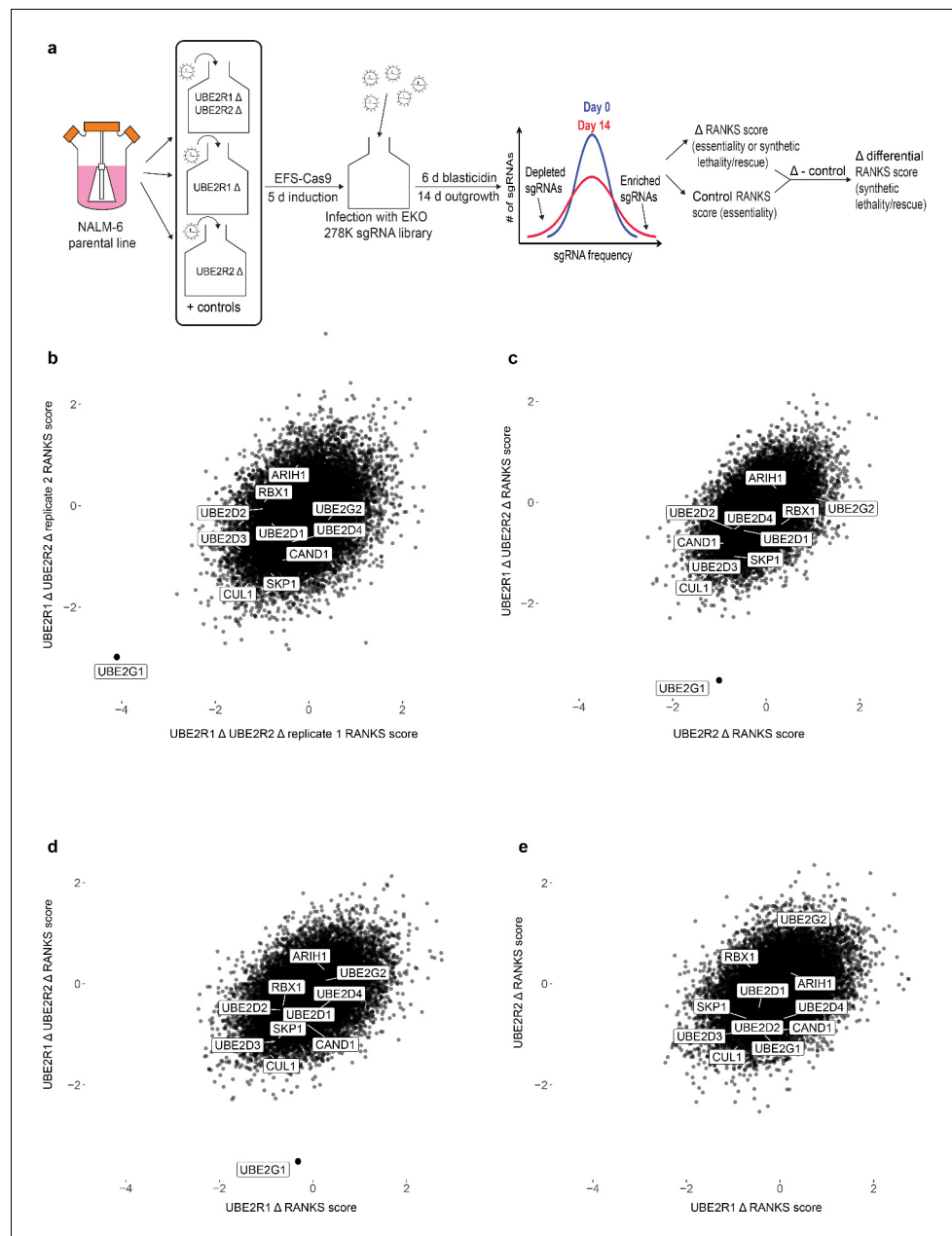
Figure 6. A genome-wide CRISPR fitness screen identifies *UBE2G1* as the primary genetic vulnerability of a *UBE2R1/2* double knockout cell line. (a) Schematic of CRISPR screen workflow to identify genes that cause synthetic lethality in a *UBE2R1/2* double mutant background. (b) Scatter plot of differential RANKS scores of all genes in replicate *UBE2R1/2* double knockout screens. Negative values indicate sgRNA depletion relative to the control population background and positive values indicate sgRNA enrichment. (c,d). Scatter plot comparisons of differential RANKS scores for *UBE2R1/2* double knockout compared to *UBE2R2* and *UBE2R1* screens. For both plots, *UBE2R1/2* scores are the average of the two screens in panel b. (e) Scatter plot comparison of *UBE2R1* versus *UBE2R2* screens. Scores for *UBE2R2* screens are the average of two independent replicates, whereas scores for *UBE2R1* are from a single screen.
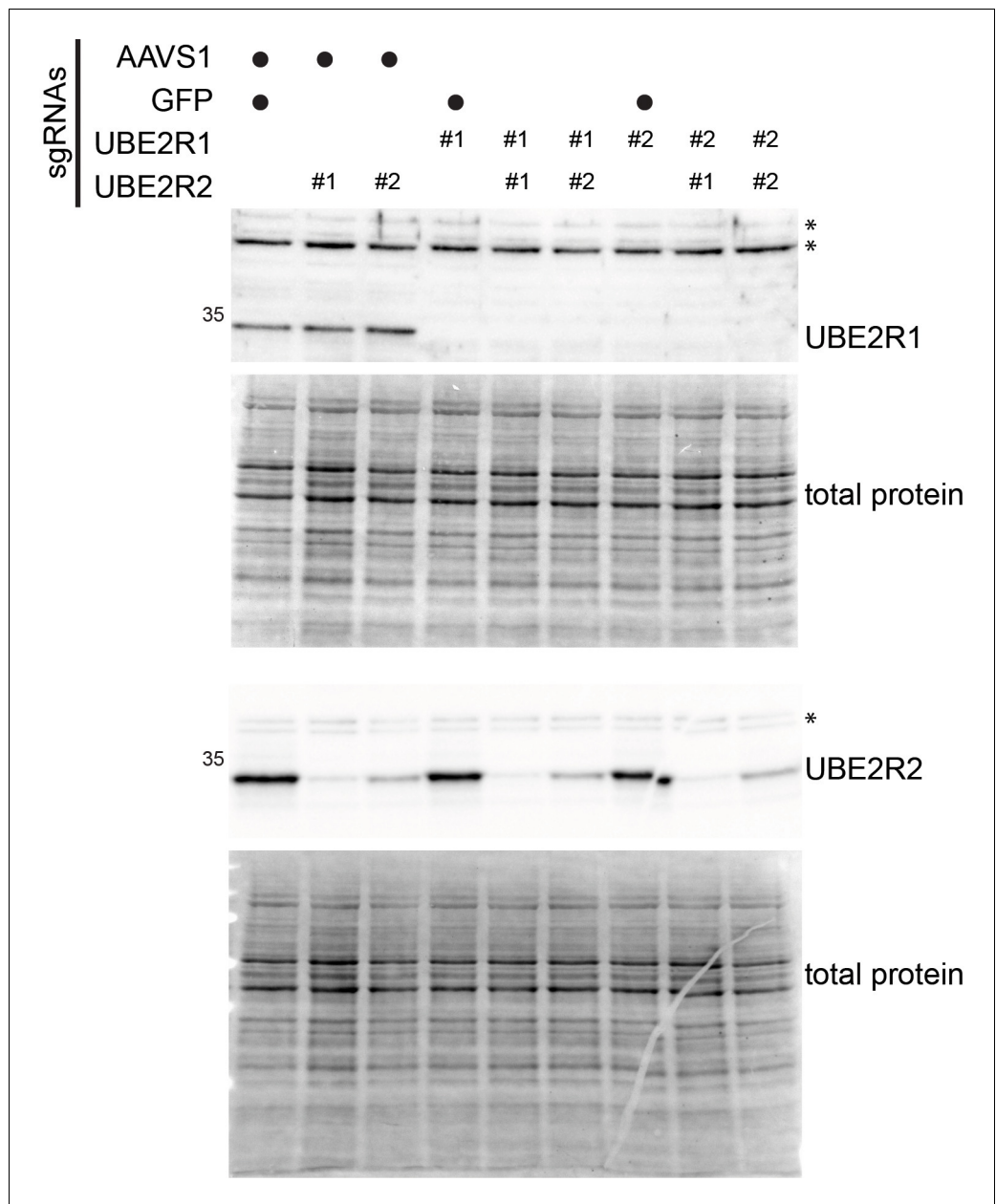
Figure 6—figure supplement 1. Knockout populations for control, *UBE2R1* and *UBE2R2* loci used in genome-wide CRISPR screens. NALM-6 populations treated with sgRNAs that target *AAVS1*, *GFP*, *UBE2R1* and/or *UBE2R2* as indicated. UBE2R1 and UBE2R2 protein were detected by immunoblot with anti-UBE2R1 or anti-UBE2R2 antibody at 1:1000 dilution. Note that since CRISPR-mediated knockout populations were not clonal, residual protein was detected in some instances.
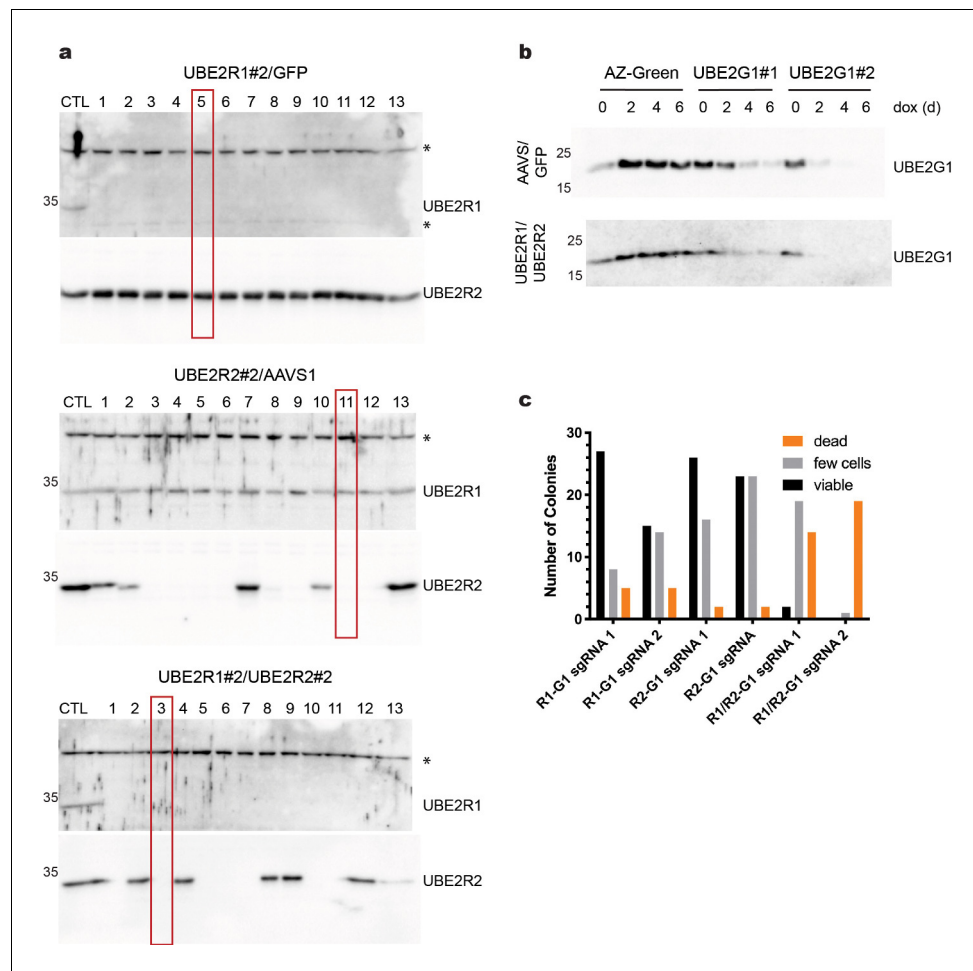
Figure 6—figure supplement 2. Proliferation defect of *UBE2R1/UBE2R2/UBE2G1* triple knockout NALM-6 cells. (a) Loss of UBE2R1 and UBE2R2 protein in clonal knockout NALM-6 cell lines for the *UBE2R1* locus (top) or *UBE2R2* locus (middle) or both loci (bottom). Clones used for analysis in panel b and c are indicated by red boxes. (b) Loss of UBE2G1 protein in *AAVS1/GFP* control and *UBE2R1/UBE2R2* double knockout NALM-6 cell lines populations treated with indicated lentiviral constructs that target either control AZ-Green or *UBE2G1*. (c) Viability of colonies for the indicated combinations of *UBE2R1*, *UBE2R2* and *UBE2G1* knockouts. All cell lines and populations for validation experiments were generated in the NALM-6 doxycycline-inducible Cas9 clone #20 background.
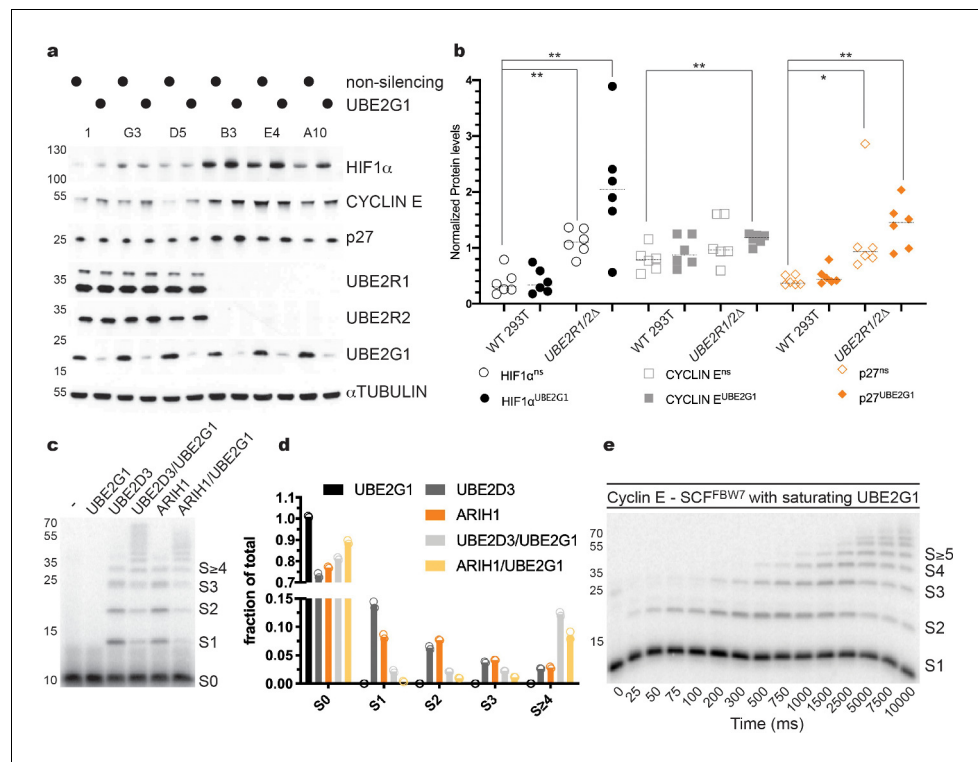
Figure 7. UBE2G1 functions redundantly with UBE2R1/2 in cells and in SCF enzyme reactions in vitro. (**a**) Comparison of the steady state stabilities of HIF1α, CYCLIN E, and p27 proteins in HEK 293T control or *UBE2R1/2* double knockout cells treated with siRNA targeting *UBE2G1* expression. (**b**) Quantitative comparison of the steady state levels for HIF1α (open or closed black circles), CYCLIN E (open or closed gray squares), and p27 protein (open or closed orange diamonds). P-values were calculated using an unpaired t-test (* and ** denote values of less than 0.05 or 0.01, respectively). P-values for all relevant combinations are provided in *Figure 7—source data 1*. Three biological replicates each for control and *UBE2R1/2* double knockout cells were used to generate the figure with duplicate technical replicates. (**c**) Representative autoradiogram of a Cyclin E peptide ubiquitylation reaction with either ARIH1, UBE2D3, or UBE2G1 alone or in combination. (**d**) Graphical representation of the levels of unmodified substrate and ubiquitylated products from the reactions shown in panel c. Duplicate technical replicates were performed to generate the figure. Source data have been provided in *Figure 7—source data 2* for panel d. (**e**) Representative autoradiogram of a Cyclin E ubiquitylation reaction with UBE2G1 levels (12.5 µM) sufficient to saturate the SCF complex. *Figure 7—figure supplement 1d* shows the fit of the data to the kinetic model. The enzyme concentrations have been provided in *Supplementary file 2*.
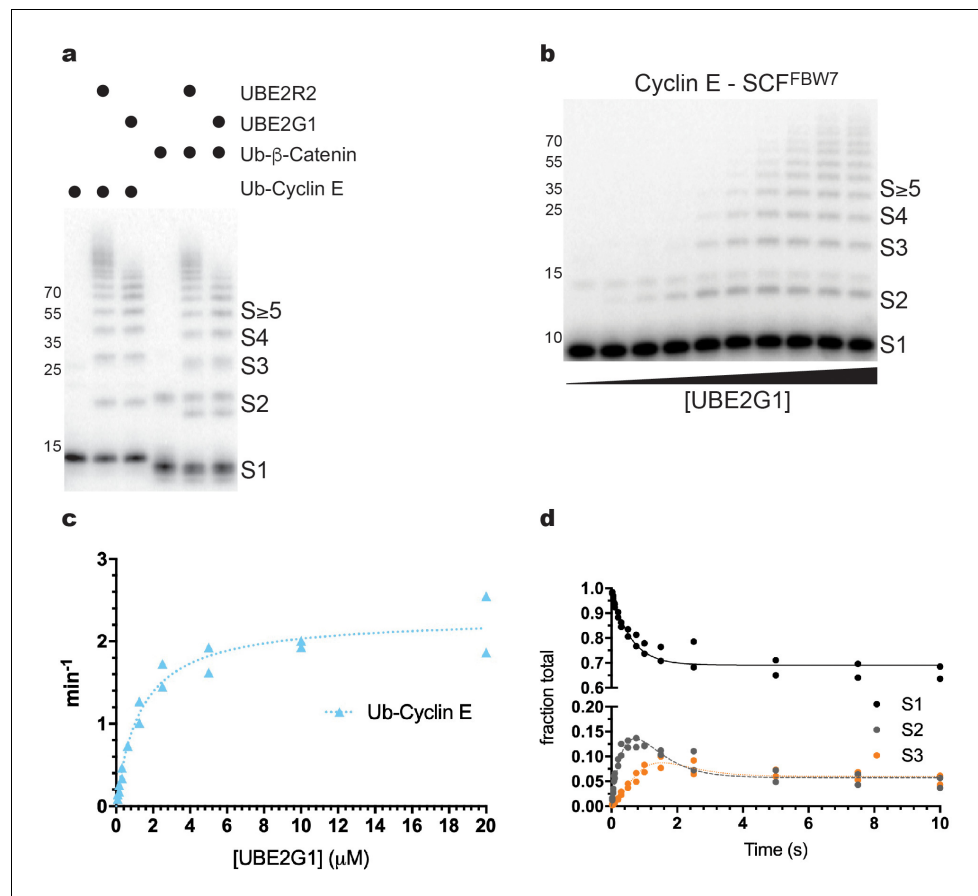
Figure 7—figure supplement 1. UBE2G1 displays robust activity in the presence of mono-ubiquitylated peptide substrates. (a) Single encounter ubiquitylation reactions containing either saturating UBE2R2 or UBE2G1 and mono-ubiquitylated β-Catenin peptide substrate and SCF^{βTRCP} or mono-ubiquitylated Cyclin E peptide substrate and SCF^{FBW7}. Reactions were quenched at 10 s (see Materials and methods). (b) Multi-turnover ubiquitylation reactions were assembled in the presence of constant amounts of SCF^{FBW7} and ^{32}P-labeled Ub-Cyclin E peptide and increasing amounts of UBE2G1 protein. Each lane represents a single ubiquitylation reaction used to calculate the reaction velocity (see Materials and methods). Representative data from two technical replicates are shown for panels (a) and (b). (c) The velocities from the reactions in (b) were plotted as a function of the UBE2G1 protein concentration and the data were fit to the Michaelis-Menten equation, $velocity = \frac{k_{cat}[S]}{([K_m + [S])}$, using nonlinear curve fitting. Data points are shown from duplicate technical replicates. (d) Data points and fit to the kinetic model of the reaction in *Figure 7d* for mono-ubiquitylated substrate. Data points are shown from duplicate technical replicates. All relevant enzyme concentrations have been provided in *Supplementary file 2*.
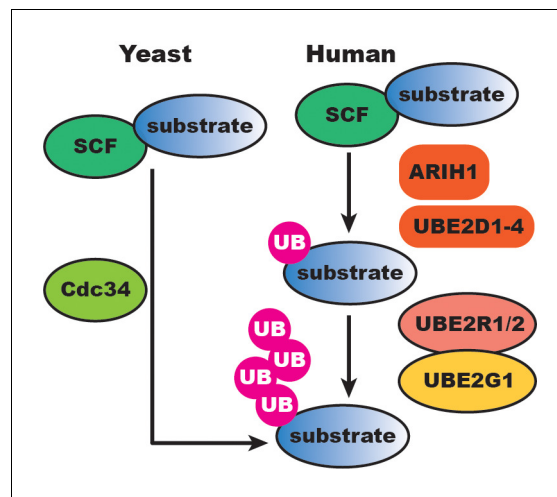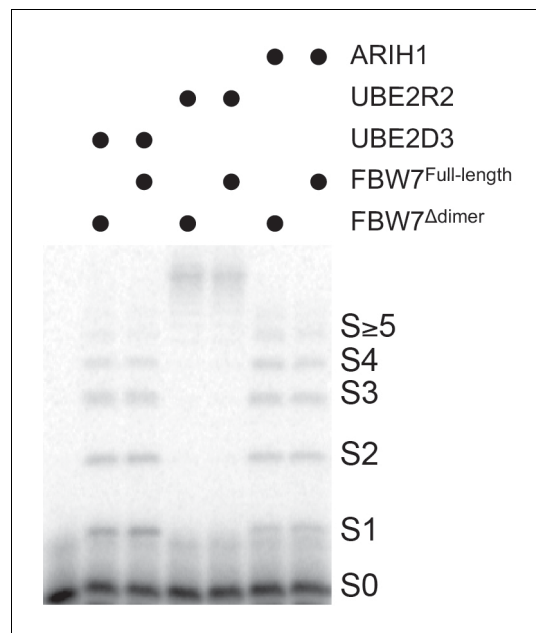
Figure 8. SCF-catalyzed substrate ubiquitylation is extensively buffered at the initiation and elongation steps in human cells compared to the simper yeast SCF system. UB, ubiquitin.

Appendix 1—figure 1. Reactions were assembled in two separate mixtures: an E1/E2 mix that contained excess unlabeled Cyclin E peptide (tube 1) and an SCF-^{32}P-labeled substrate mix (1 µM SCF, 0.2 µM substrate; tube 2). Following addition of 10 µM E2 and/or 2.5 µM ARIH1 to tube one already containing reaction buffer (30 mM Tris-HCl (pH 7.5), 100 mM NaCl, 5 mM MgCl$_2$, 2 mM DTT and 2 mM ATP), E1 (0.5 µM) and ubiquitin (80 µM), each mix was incubated at room temperature for at least 8 min. The E1/E2 mix was then pipetted into the SCF/substrate mix initiating the reaction, which was then briefly vortexed and quenched in reducing 2x loading SDS-PAGE buffer after 10 s. The reactions were resolved by SDS-PAGE and visualized by autoradiography. All reactions were performed in duplicate.
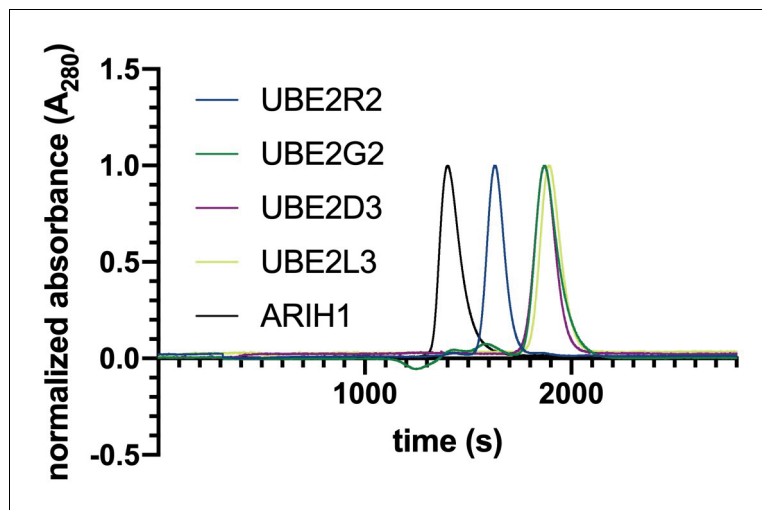
Appendix 2—figure 1. ARIH1, UBE2D3, UBE2R2, UBE2L3 and UBE2G1 all show single, monodisperse peaks by gel filtration chromatography. Purified proteins were injected onto a Superdex 75 increase 10/300 gl column that had been equilibrated in a buffer containing 30 mM Tris, pH 7.5, 100 mM NaCl, 1 mM DTT, and 10% glycerol. The absorbance at 280 nM (A_{280}) was normalized for all chromatograms.
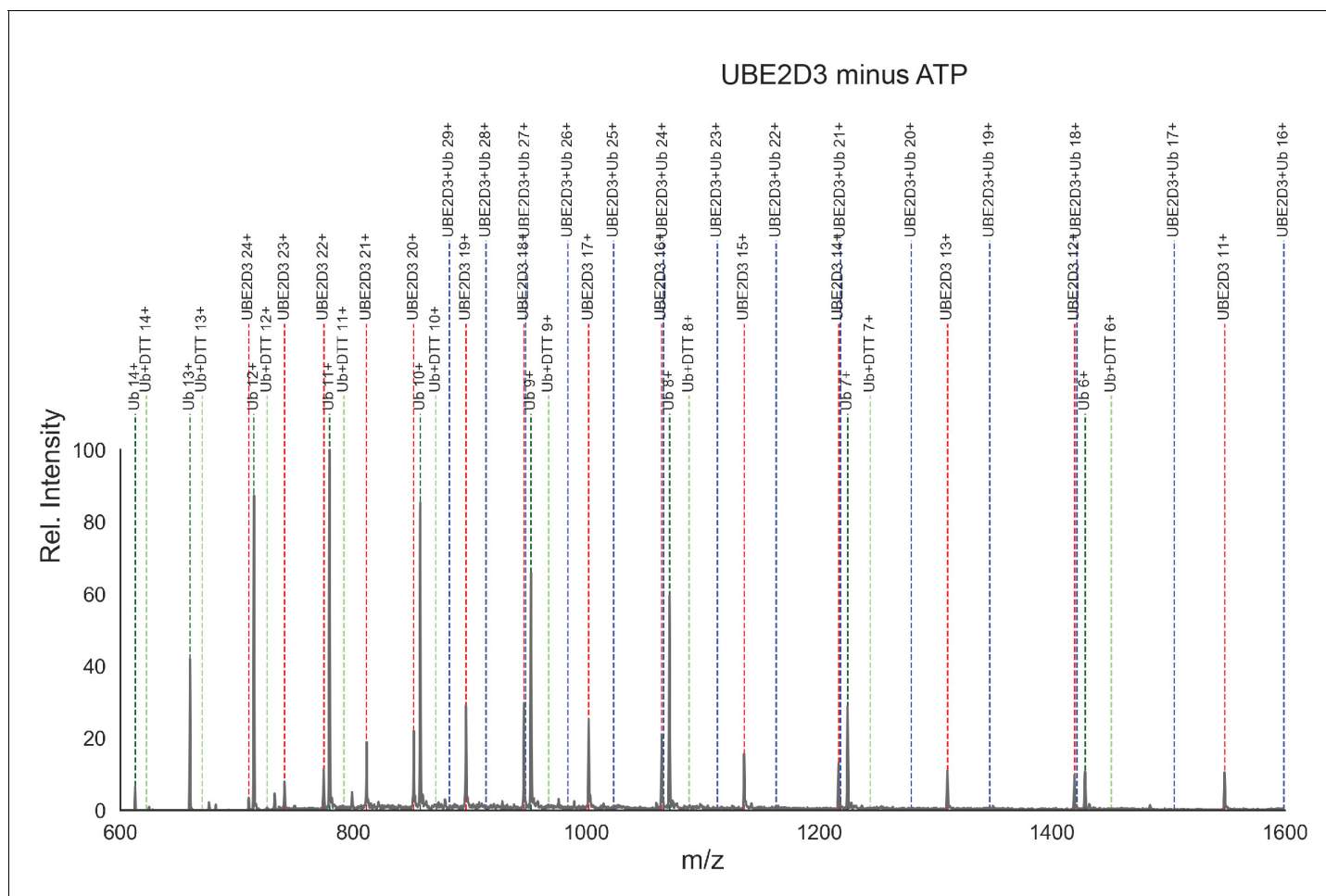
Appendix 2—figure 2. Mass spectra for control ubiquitin loading reaction containing UBE2D3. Mass spectrum for a negative control ubiquitin charging reaction containing UBE2D3 (10 μM), E1 (1 μM) and wild-type human ubiquitin (15 μm) in reaction buffer without ATP (30 mM Tris, pH 7.5, 100 mM NaCl, 5 mM MgCl₂, and 1 mM DTT). The reaction components were incubated at room temperature for 5 min, then quenched by adding 90 μL of 5% acetic acid. The detection of proteins was performed on an Agilent LC-MSD. Mass spectra were acquired in positive-ion mode, scanning from 500 to 1700 *m/z*. The electrospray voltage was set to 4 kV and the gas temperature in the spray chamber was maintained at 350℃. A stationary phase, Zorbax 300SB C3 150 mm ×2.1 mm column was used for separation (Agilent). The mobile phase A buffer was 0.2% formic acid, and the mobile phase B was 0.2% formic acid with 10% methanol and 90% acetonitrile. The flow rate was 0.2 ml min⁻¹. After a 25 min delay, the effluent was directed into the mass spectrometer. Linear gradients started with 5% mobile phase B and finished at 95% from 25 to 50 min. Data were processed using the ChemStation software package. Deconvolution of the spectra into the observed species and their abundances is shown in *Appendix 2—figure 2— source data 1* . Dotted blue lines are shown where peaks would be expected for UBE2D3 ~ ubiquitin. Notice that none were found in the absence of ATP.
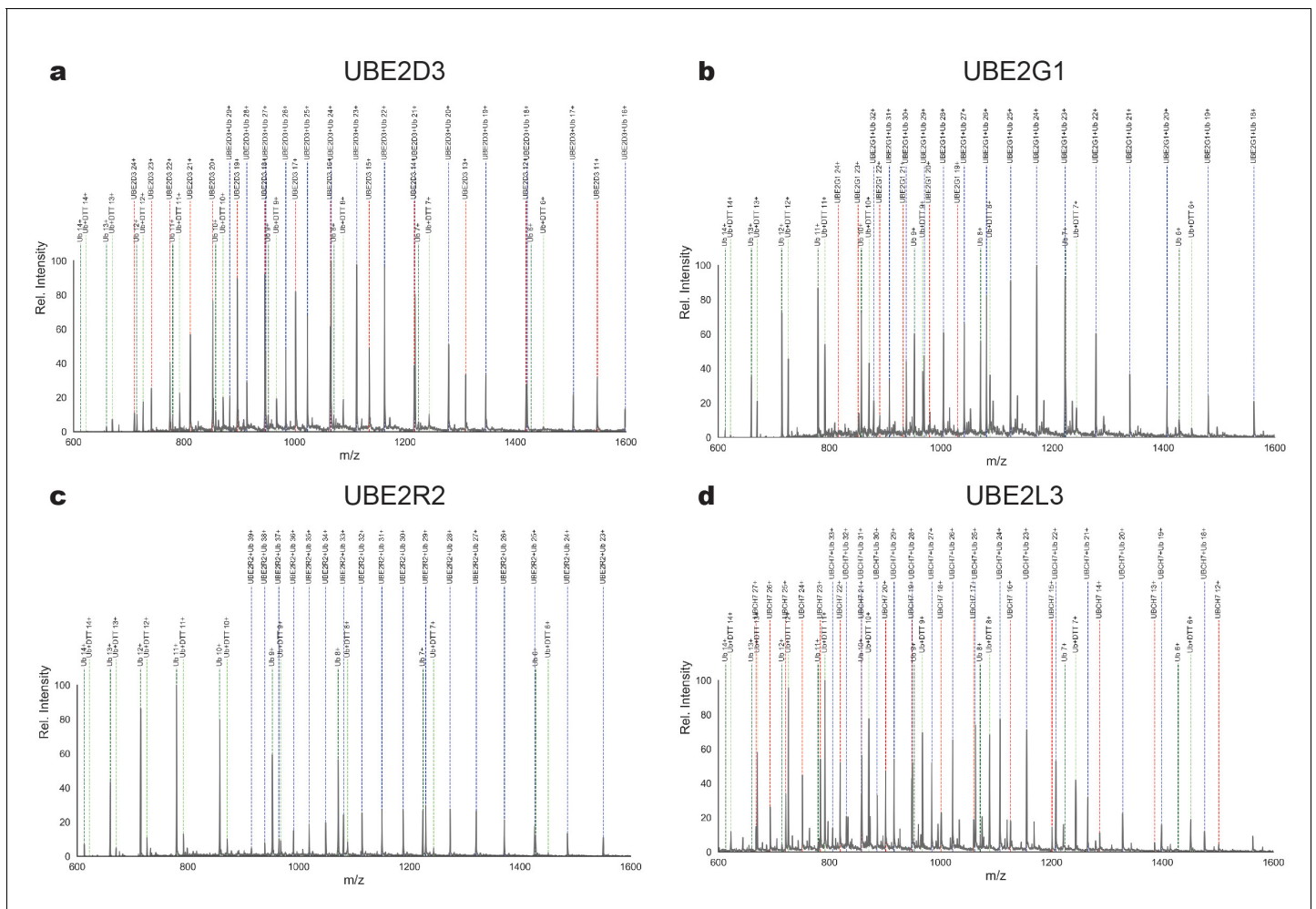
Appendix 2—figure 3. Mass spectra for ubiquitin loading reactions containing the E2s that were characterized in this study. (**a**) Same as in *Appendix 2—figure 2*, except with ATP present in the reaction buffer. (**b**) Same as (**a**), except with UBE2G1. (**c**) Same as (**a**), except with UBE2R2. (**d**) Same as (**a**), except with UBE2L3.